POLISH MARITIME RESEARCH 3 (119) 2023 Vol. 30; pp. 22-34
10.2478/pomr-2023-0036

APPLICATION OF FUEL COLD ENERGY IN CO_2 BOG RELIQUEFACTION SYSTEM ON AMMONIA-POWERED CO_2 CARRIER

Yiqun Lin
Jie Lu
Boyang Li *
Yajing Li
Qingyong Yang
College of Electromechanical Engineering, Qingdao University of Science and Technology, China

* Corresponding author: *qdlby@126.com (Boyang Li)*

ABSTRACT

A CO_2 boiled off gas (CO_2 BOG) reliquefaction system using liquid ammonia cold energy is designed to solve the problems of fuel cold energy waste and the large power consumption of the compressor in the process of CO_2 BOG reliquefaction on an ammonia-powered CO_2 carrier. Aspen HYSYS is used to simulate the calculation, and it is found that the system has lower power consumption than the existing reliquefaction method. The temperature of the heat exchanger heater-1 heat flow outlet node (node C-4) is optimised, and it is found that, with the increase of the node C-4 temperature, the power consumption of the compressor gradually increases, and the liquefaction fraction of CO_2 BOG gradually decreases. Under 85% conditions, when the ambient temperature is 0°C and the temperature of node C-4 is -9°C, the liquid fraction of CO_2 BOG reaches the maximum, which is 74.46%, and the power of Compressor-1 is the minimum, which is 40.90 kW. According to this, the optimum temperature of node C-4 under various working conditions is determined. The exergy efficiency model is established, in an 85% ship working condition with the ambient temperature of 40°C, and the exergy efficiency of the system is the maximum, reaching 59.58%. Therefore, the CO_2 BOG reliquefaction system proposed in this study could realise effective utilisation of liquid ammonia cold energy.

Keywords: mmonia-powered CO_2 carrier; liquid ammonia cold energy; CO_2 BOG; reliquefaction system; Aspen HYSYS

INTRODUCTION

In recent years, a large amount of CO_2 emission has intensified the greenhouse effect, so reducing man-made CO_2 emission has become an urgent problem to solve. Bui et al. [1], Aradottir et al. [2], and Onarheim et al. [3]considered that carbon capture and storage (CCS) is an effective method to reduce carbon dioxide emissions, so CCS technology has attracted wide attention from various industries. At present, the common storage methods are CO_2 hydrate seafloor sequestration [4], liquefied seafloor sequestration [5], mine sealing [6], ore carbonisation [7] and so on. In this study, the liquefaction method in the liquefaction seafloor storage will be studied. Usually when CO_2 is sequestered, it needs to be transported across regions and countries to specific locations for sequestering, for example, in Iceland, where storage capacity is high [8], but for the long-distance transport of liquefied carbon dioxide (LCO_2), ship transportation is a better choice than pipeline transportation [9].

LCO_2 is usually transported on ships by placing storage tanks in the ship's cargo hold, so the temperature and pressure for LCO_2 transport should be considered. Hegerland [5] points out that, in order to reduce the investment cost of the LCO_2 storage tanks, it is necessary to get as close to the triple point of CO_2 as

possible (5.17 bar, -56.6℃). However, in practical engineering applications, the temperature of the LCO_2 should not be lower than -50℃, because when the temperature and pressure are close to the triple point of CO_2 [10], LCO_2 easily forms dry ice, which will lead to the risk of pipeline blockage. Due to the low storage and transportation temperature of LCO_2, there is a large temperature difference with the outside environment, so the LCO_2 storage tank will generate infiltration heat, which leads to CO_2 boiled off gas (CO_2 BOG). In order to reduce the infiltration heat, it is necessary to add an insulation layer on the LCO_2 storage tank, but there is still a large temperature difference between the tank and the outside environment and it still generates infiltration heat, with the result that the LCO_2 produces a small amount of BOG. Due to the long route and sailing time of CO_2 carriers, more and more CO_2 BOG will be generated. If the CO_2 BOG is not processed and is directly discharged into the atmosphere, it will also contribute further to the greenhouse effect. Therefore, a CO_2 reliquefaction system must be set up on CO_2 carriers to reliquefy a small amount of CO_2 BOG [11].

More and more scholars are looking for new technologies to apply for BOG reliquefaction on ships [12]]. Alabdulkarem et al. [13] carried out research on the CO_2 liquefaction process and proposed to use NH3 as the refrigerant, which can reduce the energy consumption of the CO_2 reliquefaction system. Other scholars have also studied more novel methods, such as absorption refrigeration [14] and turbine expander applications [15]. Seo et al. [16] proposed four different CO_2 liquefaction systems and determined their design parameters through multiple process simulations and optimisation. Decarre et al. [17] proposed a CO_2 liquefaction process using two cooling cycles and a reliquefaction system. Duan et al. [18] proposed a liquefaction method that uses waste heat to drive ammonia refrigeration, and then uses a booster pump to achieve CO_2 supercharging. Zahid et al. [19] proposed a new method of CO_2 liquefaction with low energy consumption. Awoyomi et al. [20] proposed the use of a two-stage reliquefaction cycle to recover evaporated gas and capture emitted carbon dioxide. Sang and Min [21] and Deng et al. [22]] studied the influence of impurities on the CO_2 BOG reliquefaction system, and concluded that impurities may increase the risk of the system reliquefaction and affect the cost of CO_2 liquefaction; the cost of liquefaction is lower for pure CO_2, and 34% higher for CO_2 containing impurities Y. Lee et al. [23] studied the reliquefaction characteristics of CO_2 and proposed a feasible scheme for a CO_2 BOG reliquefaction process suitable for large carriers, which is conducive to the further development of liquefied CO_2 carriers. Muhammad et al. [24] proposed a CO_2 liquefaction system and found that a lower pressure and cooling temperature could improve the system performance. A CO_2 BOG reliquefaction system will consume a large amount of energy, and a research focus in the industry is now to seek a method to reduce the energy consumption of ships [25]. Therefore, it is particularly important to find a method to reduce the energy consumption of CO_2 BOG reliquefaction.

In recent years, in order to reduce the emission of ship exhaust pollutants, the International Maritime Organization (IMO) has put forward increasingly strict ship exhaust emission policies [26], in which clean fuels such as ammonia [27], LNG [28], and hydrogen [29] keep emerging. Frankl et al. [30] and Mounaim-Rousselle et al. [31] proposed that the combustion of ammonia fuel can achieve "zero carbon" emission, making it undoubtedly a more ideal carbon-free fuel for CO_2 carriers. Ammonia fuel is usually stored on the ship in the form of low-temperature liquid (liquid ammonia), and the storage temperature is -33.5℃ [32]. Liquid ammonia fuel needs to be heated to the supply temperature of the ship's main engine before being used. In this process, the ammonia fuel will release cold energy, but most of this cannot be fully utilised and is therefore wasted. Liquid ammonia has just started to be used as a clean marine fuel and has not been widely used, and research on the utilisation technology of liquid ammonia cold energy is relatively scarce. In addition, the cold energy released by liquid ammonia fuel is relatively small. Therefore, how to make full use of this part of the cold energy is another research hotspot in the industry.

As cold energy is required to reliquefy the small amount of CO_2 BOG produced by an ammonia-powered CO_2 carrier, the cold energy released on the carrier can therefore be used in the CO_2 BOG reliquefaction process. However, the temperature of liquid ammonia is -33.5℃, which may be higher than that of LCO_2 under different transport temperatures. Therefore, it is urgent to find a solution that can use liquid ammonia cold energy in the CO_2 reliquefaction process on CO_2 carriers.

In this study, it is proposed to utilise the liquid ammonia cold energy of the CO_2 BOG reliquefaction process in an ammonia-powered CO_2 carrier, which can not only greatly reduce the power consumption in the process of reliquefaction, but also make full use of the ammonia fuel cold energy released by the carrier, thus solving the problem of wasting this cold energy. This makes the super environment-friendly ammonia-powered CO_2 carrier more in line with the requirements of energy conservation and emission reduction. In this study, a CO_2 BOG reliquefaction system using liquid ammonia cold energy is first proposed. The process and numerical calculation are carried out for the system using Aspen HYSYS, the parameter optimisation of the system is completed, and the node parameters affecting the heat exchanger heat transfer rate, the compressor power consumption and the liquefaction fraction rate of CO_2 BOG are optimised. An exergy efficiency model is established to verify the feasibility of the system, and can provide a theoretical basis and technical support for large-scale application in ammonia-powered CO_2 carriers in the future.

RESEARCH BASIS

ESTABLISHMENT OF MODEL

The CO_2 carrier of a shipyard in China is selected as the research object. Its conceptual ship model is shown in Fig. 1. The main engine power of the ship is 15,000 kW, the ship can carry 50,000 m^3 of LCO_2, and liquid ammonia is used as fuel. Other parameters of the ship are shown in Table 1.

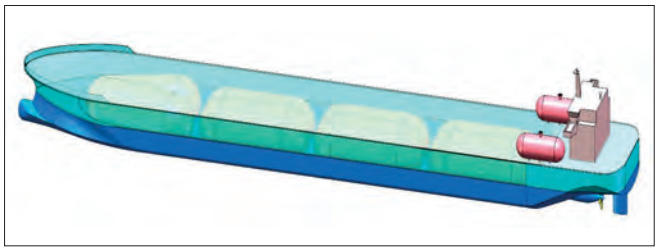

Fig. 1. Research object model diagram

Tab. 1 Main parameters of the CO_2 carrier

Parameter	Value	Parameter	Value
Length overall (m)	230.15	Draft (m)	13.5
Breadth moulded (m)	31.6	Loading (m³)	50780.7
Depth (m)	21.9	Main engine power (kW)	15000
Pressure of LCO2 (kPa)	659	Cargo hold temperature (°C)	-50

At a certain temperature, CO_2 is in liquid state when it reaches the saturation pressure of CO_2 at this temperature. At different temperatures, the liquefaction pressure of CO_2 is different, and the corresponding relationship between the saturation pressure and temperature is shown in Fig. 2.

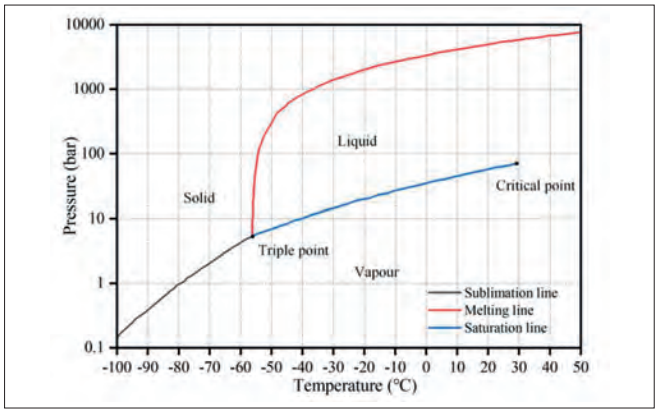

Fig. 2. Phase diagram of CO_2 pressure and temperature

As can be seen from Fig. 2, when the temperature of the CO_2 is less than -40°C, its saturation pressure is less than 10 bar; when the temperature is more than -40°C, the saturation pressure is more than 10 bar. A higher saturation temperature can reduce the cold energy required for CO_2 liquefaction, but a higher temperature requires a higher transport pressure. Thus, this means a higher requirement on the pressure of the LCO_2 storage tank. Usually, the temperature range of LCO_2 transported by ships is -50 ~ -20°C [11], and the corresponding saturation pressure is 6.59 ~19.7 bar. In addition, the density of LCO_2 is different at different transport temperatures, which will also affect the transport volume of the LCO_2. Its density can be calculated by Aspen HYSYS when the temperature is between -50°C and -20°C (5°C is a temperature gradient). Li and Yan [33] proposed that the Peng–Robinson (PR) and Soave–Redlich–Kwong (SRK) equations of state can both be used to calculate the saturation pressure, and the average absolute deviation compared with the actual measured data is less than 3%. However, SRK should be excluded during liquefaction and reliquefaction as they are not recommended if the temperature is below 290 K. Therefore, in this study, the PR equation of state is adopted and the results are summarised in Table 2.

Tab. 2. LCO_2 density at different temperatures

Temperature (°C)	-50	-45	-40	-35	-30	-25	-20
Density (kg/m³)	1151	1132	1114	1094	1074	1053	1031

As can be seen from Table 2, as the liquefaction temperature of the CO_2 increases, its density gradually decreases. Compared with low transport temperature, to transport the same mass of LCO_2, a larger tank volume is required at a high transport temperature, which increases the investment cost of tank construction. Irrespective of low- or high-temperature transportation, there is still a large temperature difference between the temperature of the LCO_2 and the ambient temperature, and the existence of infiltration heat will cause the evaporation of LCO_2. In order to reduce the evaporation, it is still necessary to add an insulating layer on the LCO_2 tank. Therefore, compared with low-temperature transportation, the insulating layer does not decrease but, on the contrary, increases the cost, with the requirement for the tank to have a greater bearing capacity. Since the LCO_2 storage temperature on land is -20.0°C [34], and on ships is roughly between -50°C and -20.0°C, considering the density of LCO_2, the higher the temperature, the lower the density, so the tank at -50.0°C may be more advantageous than at -20.0°C. That is, the amount of LCO_2 stored per unit of storage volume can be increased by 12%. The transport temperature of -50°C and the transport pressure of 6.59 bar are used in this study. Y. Lee et al. [23] and Engel et al. [35] also proposed that a -50°C transport temperature is desirable.

PREREQUISITES

Although the insulating layer is added to the LCO_2 storage tank, due to the large temperature difference between the inside and outside of the tank, the LCO_2 in the tank will still have heat exchange with the outside air, generating infiltration heat and resulting in the generation of CO_2 BOG. However, the volume of the storage tank is fixed. If there is more CO_2 BOG, the pressure in the storage tank will be too high and can easily cause damage to the tank, so the CO_2 BOG should be treated or released. If it is discharged directly into the atmosphere, it will aggravate the greenhouse effect, so it should instead be reliquefied.

Based on the route characteristics of the ammonia-powered LCO_2 carrier, the external ambient temperature of the storage tank varies greatly during the voyage. Under different external ambient temperatures, the amount of CO_2 BOG in the storage tank is different. In order to calculate the amount of CO_2 BOG in the tank under different external environments, a variety of ambient temperatures are selected in this study, which are 0°C, 10°C, 20°C, 30°C and 40°C, respectively, and the amount of CO_2 BOG under the different ambient temperatures is calculated. The calculation method is as follows:

(1) Calculation of heat transfer coefficient k

Heat transfer coefficient k:

$$k = \frac{1}{\frac{1}{h_w} + \frac{\delta_i}{\lambda_i} + \frac{1}{h_n}} \quad (1)$$

In the formula,

h_n is the heat transfer coefficient of the inner wall, W/(m²·k).

It is calculated as follows: the LCO_2 storage tank is made of 5Ni steel with a thickness of 7 mm and the temperature inside the tank is -50°C. The data in Table 3 are the heat conduction coefficient of the 5Ni steel at different temperatures [36]. The heat conduction coefficient of the tank inner wall can be calculated by interpolation.

Tab. 3. Heat conduction coefficient of 5Ni steel at different temperatures

Temperature (k)	75.15	97.15	103.2	120.2	151.2	201.2	251.2	300.2
Heat conduction coefficient (W/(m))	13.1	16.1	17.3	19.3	21	24.8	27.4	29.2

The heat conduction coefficient of the storage tank inner wall is as follows:

$$\frac{(27.4-24.8)\times(223-201.2)}{251.2-201.2} + 24.8 = 25.93 \text{ W/(m}\cdot k)$$

The thickness of the storage tank is designed as 7 mm, and the heat transfer coefficient of the inner wall can be calculated:

$$h_n = \frac{25.93}{0.007} = 3704.29 \text{ W/(m}^2\cdot k)$$

h_w is the convective heat transfer coefficient of the outer wall, W/(m²·k).

Using the same method, taking the external temperature of 20°C as an example, the thermal conductivity of the tank outer wall can be calculated:

$$\frac{(29.2-27.4)\times(293-251.2)}{300.20-251.20} + 27.4 = 28.94 \text{ W/(m}\cdot k)$$

Thus, the heat transfer coefficient of the tank outer wall can be calculated:

$$h_w = \frac{28.94}{0.007} = = 4134.29 \text{ W/(m}^2\cdot k)$$

δ_i is the thickness of the thermal insulation material.

The thickness of the insulation layer of the LCO_2 tank is usually 80 ~ 120 mm. In this study, the thickness of the insulation layer is 100 mm.

λ_i is the heat conductivity coefficient of the thermal insulation material, W/(), 0.02 W/(m·k).

The insulation material is the commonly used rigid polyurethane foam, which has a good insulation effect and low heat conductivity of only 0.018~0.024 W/(m·k). In this article, the value is 0.02 W/(m·k), which is obtained through actual investigation.

Through calculation, the heat transfer coefficient k can be calculated:

$$k = \frac{1}{\frac{1}{h_w} + \frac{\delta_i}{\lambda_i} + \frac{1}{h_n}} = \frac{1}{\frac{1}{4134.29} + \frac{0.1}{0.02} + \frac{1}{3704.29}} =$$

$$= 0.199 \text{W/(m}^2\cdot k)$$

Since the value of h_w has little influence on the total heat transfer coefficient k, when the external temperatures are 0°C, 10°C, 30°C and 40°C, respectively, the value of the total heat transfer coefficient k remains unchanged at 0.199 W/(m²·k), so this value will be used in subsequent calculations.

(2) Calculation of heat transfer rate Q

$$Q = A \cdot k \cdot \frac{\Delta T}{1000} \quad (2)$$

In the formula,

A – is the surface area of the tank, m³;

k – is the heat transfer coefficient, W/(m²·k);

Q – is the total heat transfer rate of the tank, kW.

(3) Calculation of evaporation rate R

$$R = \frac{Q\times 24\times 3600}{r\times V\times \rho} \quad (3)$$

In the formula,

r – is the vaporisation heat of LCO_2, kJ/kg, here 339.737 kJ/kg [20];

V – is the volume of the tank, m³, and taken in this study as 50780.707 m³;

ρ – is the density of LCO_2 at -50°C, kg/m³, here 1151 kg/m³;

R – is the evaporation rate of LCO_2, %.

(4) Calculation of evaporation capacity Q_{BOG}

$$Q_{BOG} = \frac{v\rho R}{24} \quad (4)$$

Eqs. (1)~(4) can be used to calculate the amount of CO_2 BOG at different ambient temperatures, and the results are summarised in Table 4.

Tab. 4. Amount of CO_2 BOG at different ambient temperatures

Ambient temperature (°C)	0	10	20	30	40
Evaporation capacity (kg/h)	1299.86	1559.90	1819.83	2079.76	2339.80

DESIGN OF CO_2 BOG RELIQUEFACTION SCHEME

COMPARISON SCHEME

Recently, some scholars have studied using seawater as a cold source for CO_2 BOG reliquefaction [37]. However, the temperature of seawater is higher and so also is the corresponding liquefaction pressure of CO_2. Whether single-stage or multistage compression is adopted, the power consumption of the refrigeration compressor is greater. In addition, the temperature difference between the liquefaction temperature of CO_2 BOG

using seawater as a cold source and the transport temperature of LCO_2 is large, so the LCO_2 needs to be expanded and cooled after liquefaction. However, when the temperature difference is large, the expanded LCO_2 will partially vaporise, resulting in a low liquefaction fraction of CO_2 BOG. The CO_2 BOG reliquefaction system with seawater as the cold source is shown in Fig. 3. It is necessary to compress the CO_2 BOG to the saturation pressure (57.26 bar) corresponding to CO_2 at a temperature higher than that of seawater (20°C). Due to the large compression ratio of the compressor, in order to save compressor power consumption, the method of multistage compression is adopted to realise the liquefaction of the CO_2.

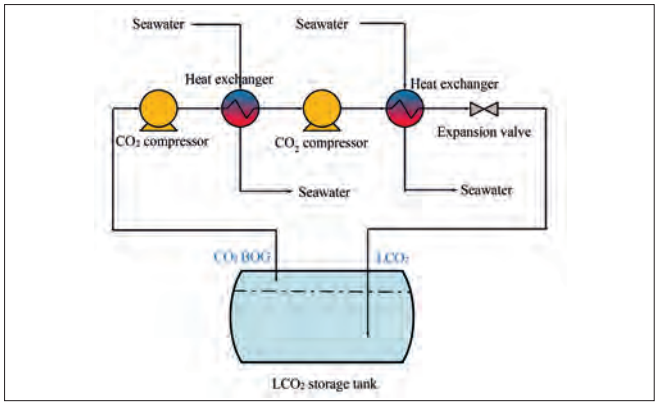

Fig. 3. System diagram of CO_2 BOG liquefaction process

Aspen HYSYS simulation software was used to simulate the liquefaction system in Fig. 3. The setting of the node parameters refers to part of the data in the literature [37], and the flow of CO_2 BOG adopts the calculated value of CO_2 BOG when the external temperature is 20°C in Table 4, which is 1819.83 kg/h. The simulation system diagram and the parameter settings of the key nodes are shown in Fig. 4. Through simulation, it can be obtained that the power consumption of compressor K-1 is 73.36 kW, and compressor K-2 is 28.67 kW, so the total power consumption of the compressor is 102.03 kW. In addition, the vaporisation fraction of node 6 is 51.58%, and the liquefaction fraction rate is only 48.42%.

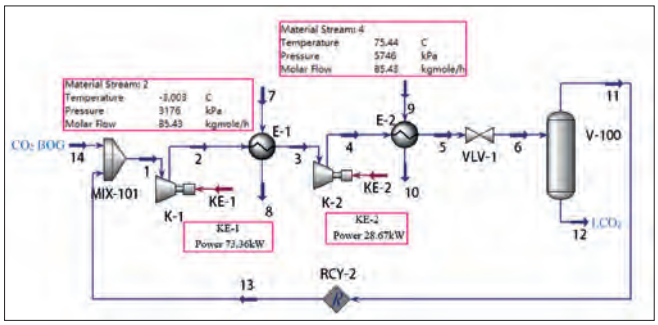

Fig. 4. System simulation diagram of comparison scheme

DESIGN OF CO_2 BOG RELIQUEFACTION SCHEME WITH LIQUID AMMONIA AS COLD SOURCE

According to the above calculation, the main power consumption in the CO_2 BOG reliquefaction system is by the compressor. To reduce this, it is necessary to reduce the compression ratio of the compressor. The temperature of liquid ammonia is -33.5°C. If it can be used as the cold source of CO_2 BOG reliquefaction, the liquefaction temperature can be reduced, and thus the liquefaction pressure and the power consumption can also be reduced. Based on this, a system that utilises liquid ammonia cold energy in the process of CO_2 reliquefaction is proposed, as shown in Fig. 5.

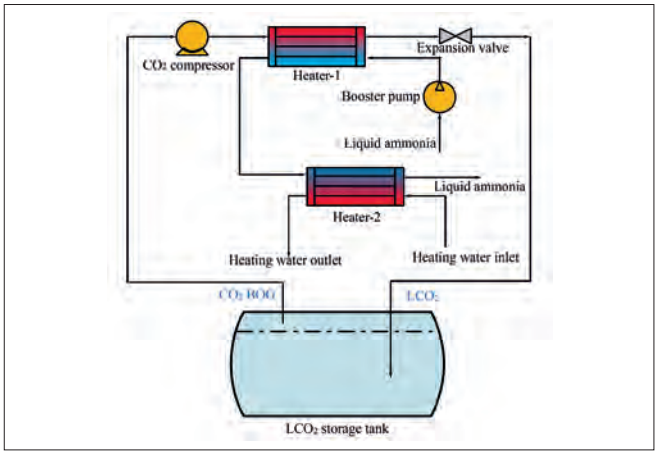

Fig. 5. CO_2 BOG reliquefaction system with liquid ammonia as cold source

The system working principle is as follows: CO_2 BOG produced by the LCO_2 storage tank is first pressurised by the compressor and then enters the heat exchanger Heater-1 to realise liquefaction by using the liquid ammonia cold energy. LCO_2 is a high pressure liquid after liquefaction. In order to meet the storage conditions of the LCO_2, an expansion valve is needed to expand the LCO_2 pressure to the storage pressure and temperature. Then the LCO_2 is returned to the LCO_2 storage tank; liquid ammonia is first supercharged to 80 bar by the booster pump, and then heated by the heat exchanger Heater-1 to release cold energy. However, the temperature of the liquid ammonia still cannot meet the supply temperature of the ship's main engine, so it needs to be heated by the heat exchanger Heater-2 using cylinder liner water heated to about 40°C.

SIMULATION CALCULATION AND RESULTS

The ship uses liquid ammonia as fuel, the calorific value of which is only 18.568 MJ/kg, but the power of the ship's main engine is higher, so it needs a greater ammonia fuel supply. In different ship operating conditions, the supply of liquid ammonia fuel is different, so the cold energy released is also different. In order to study the cold energy release of liquid ammonia under various ship conditions, 55%, 65%, 75%, 80%, and 85% ship working conditions are taken as examples. The amount of liquid ammonia fuel supplied can be calculated, and the results are summarised in Table 5.

Tab. 5. Amount of liquid ammonia fuel supplied under different working conditions

Working condition (%)	55%	65%	75%	80%	85%
Amount of liquid ammonia (kg/h)	3359	3969.7	4580.5	4885.8	5191.2

Based on the system diagram in Fig. 5, a simulation flow diagram is created using Aspen HYSYS, as shown in Fig. 6. In this simulation, the NBS steam equation is selected as the physical property method for the cylinder liner heating water in the system, and the P–R equation is selected as the physical property method for other fluid components. The efficiency of the pump is set at 85%. In this simulation, the entire process is assumed to be static and stable.

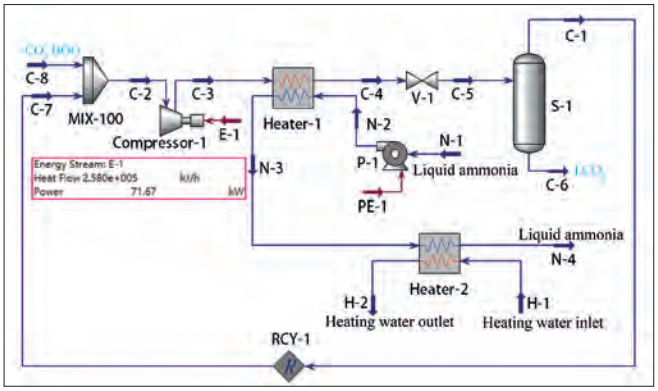

Fig. 6. Simulation system diagram of liquid ammonia as cold source in CO_2 BOG reliquefaction process

Taking the 85% ship working condition and the ambient temperature of 20°C as an example, the parameters of the simulation system in Fig. 6 are set. It can be seen from Table 4 that when the ambient temperature is 20°C, the amount of CO_2 BOG is 1819.83 kg/h, so the flow of node C-2 is set to 1819.83 kg/h. As can be seen from Table 5, when the ship working condition is 85%, the liquid ammonia supply is 5191.2 kg/h, so the flow of node N-1 is set at 5191.2 kg/h. The liquefaction pressure of node C-4 can be calculated according to the liquefaction temperature of node C-4, so as to figure out the pressure of node C-3. The liquefaction temperature of node C-4 is mainly related to the flow of LCO_2 and liquid ammonia, but the temperature of node C-4 should be selected within a range that ensures that no temperature crossing occurs in heat exchanger Heater-1. In order to ensure the normal operation of the simulation system, the temperature of node C-4 is initially selected as -2°C. The settings of the other main simulation parameters are shown in Table 6, and the simulation results of the main nodes are shown in Table 7.

Tab. 6. Setting of main simulation parameters

Nodes	C-2	C-4	C-5	N-1	N-2	N-4	H-1	H-2
Fluid	CO_2	CO_2	CO_2	LNH_3	LNH_3	LNH_3	H_2O	H_2O
Temperature (°C)	-50	-2	-	-33.5	-	40	80	68
Pressure (kPa)	659	-	659	200	8040	-	200	-
Mass flow (kg/h)	1820	-	-	5191	-	-	-	-

By comparing the simulation results of the two systems in Fig. 4 and Fig. 6, it can be found that, when the CO_2 BOG flow is the same, using the liquefaction system shown in Figure 5, the vaporisation fraction of CO_2 is lower, the vaporisation fraction is 30.78% and the liquefaction fraction is 69.22%. In the system,

Tab. 7. Main node simulation results

Nodes	Fluid	Temperature (°C)	Pressure (kPa)	Mass flow (kg/h)	Vapour fraction (%)
C-1	CO_2	-50	659	809.3	100
C-3	CO_2	80.64	3285	2629	100
C-4	LCO_2	-2	3265	2629	0
C-5	CO_2/LCO_2	-50	659	1820	30.78
C-6	LCO_2	-50	659	1820	0
N-1	LNH_3	-33.5	200	5191	0
N-2	LNH_3	-31.82	8040	5191	0
N-3	LNH_3	5.859	8020	5191	0
N-4	LNH_3	40	8000	5191	0
H-1	H_2O	80	200	22540	0
H-2	H_2O	68	500	22540	0

the main power consumption is by Compressor-1, which can be calculated as 71.67 kW by simulation. The compressor power consumption comparison scheme is 102.03 kW. Therefore, the compressor consumes less power in the CO_2 BOG reliquefaction system using liquid ammonia cold energy. This is because, compared with seawater, when using liquid ammonia cold energy the cold source temperature is lower, the liquefaction temperature and saturation pressure corresponding to CO_2 BOG are lower, and the power consumption of the compressor is also lower. In this simulation, the temperature of node C-4 is randomly selected under the condition that temperature crossing does not occur in heat exchanger Heater-1. The corresponding temperature may not be the temperature where the system cold energy is fully utilised and the compressor power consumption is minimal. Therefore, the temperature of node C-4 should be optimised.

RESULT OPTIMISATION

ANALYSIS OF HEAT TRANSFER RATE

When the working condition of the ship is constant, the supply of liquid ammonia fuel is constant. Therefore, the heat transfer rate of Heater-1 indicates the amount of liquid ammonia cold energy that can be used. The heat transfer rate of the heat exchanger is related to the heat exchange temperature difference. For cold flow and heat flow of Heater-1, the temperature of node N-2 (Heater-1 cold flow inlet) is determined according to the temperature of node N-1 (liquid ammonia fuel imports) and the pressure of node N-2. The temperature of node N-1 is equal to the liquid ammonia temperature, so the pressure and temperature of node N-2 are determined. The temperature of node C-3 (Heater-1 heat flow inlet) and N-3 (Heater-1 cold flow outlet) is determined according to the temperature of node C-4 (Heater-1 heat flow outlet). Therefore, the temperature difference of the hot and cold flow of Heater-1 mainly depends on the

temperature of node C-4, which may affect the heat transfer rate of Heater-1. Under a certain ship working condition, with different ambient temperatures, the influence of the node C-4 temperature on Heater-1 is studied by changing the temperature of node C-4. Taking the 85% ship working condition as an example, simulation calculation is carried out for the CO_2 BOG reliquefaction system with liquid ammonia cold energy under different external ambient temperatures, so as to study the heat transfer of Heater-1 under the different temperatures. According to these different temperatures, different node C-4 temperatures are then selected. Under the condition that no temperature crossing occurs in Heater-1, five different temperatures of node C-4 are taken, respectively, including the lowest temperature of node C-4 on the premise of ensuring the normal operation of the heat exchanger. The results are summarised in Fig. 7.

Suppose the heat transfer rate of the heat exchanger is expressed in Q (kJ/h), $Q = LMTD \cdot UA$, where $LMTD$ (°C) is the logarithmic mean temperature difference of the cold flow and heat flow of the heat exchanger and UA (kJ/°C*h) represents the total heat transfer coefficient. As can be seen from Fig. 7 (a)~(e), with the increase of the node C-4 temperature, the LMTD value of Heater-1 is increasing. This is because, as the node C-4 temperature increases, the temperature difference between the heat flow and cold flow also increases, so the value of LMTD increases. In addition, as the temperature of node C-4 increases, the heat transfer rate of Heater-1 gradually decreases, and according to the formula $Q = LMTD \cdot UA$, as the temperature of node C-4 increases, the value of UA becomes smaller and smaller. It can be seen that the decrease of temperature of node C-4 will increase the heat transfer rate of Heater-1. Under 85% ship working conditions, when the ambient temperature is 0°C and the temperature of node C-4 is -5°C, the heat transfer rate of Heater-1 is the smallest, at 4.46×10^5 kJ/h. When the external ambient temperature is 40°C and the temperature of node C-4 is 3°C, the heat transfer rate of Heater-1 is the highest, at 7.96×10^5 kJ/h.

RELATIONSHIP BETWEEN COMPRESSOR POWER, CO_2 BOG LIQUID FRACTION AND C-4 TEMPERATURE

The temperature of node C-4 is the liquefaction temperature of CO_2 BOG, and the liquefaction pressure of node C-4 can be calculated according to the temperature of node C-4. The pressure drop of Heater-1 is 20 kPa, so the pressure of node C-3

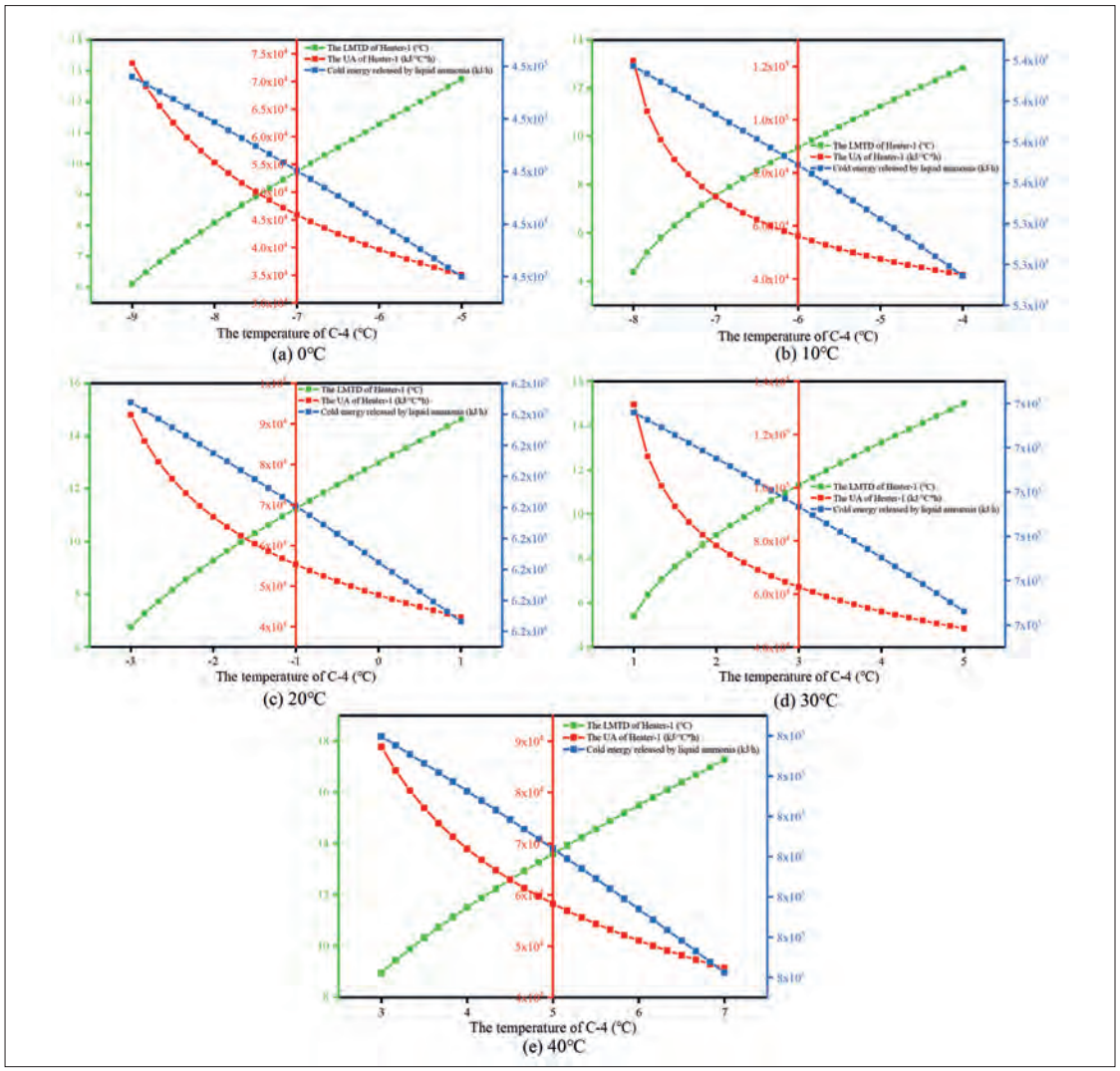

Fig. 7. Variation curves of heat transfer rate of Heater-1 and node C-4 temperature

and compressor power consumption can be calculated, and the compressor power consumption is related to the temperature of node C-4. Meanwhile, at node C-4, the LCO_2 is at high pressure and low temperature, but the temperature is still higher than the storage temperature of LCO_2. In order to meet the storage conditions, it is necessary to expand and cool the LCO_2. After passing through the expansion valve V-1, both the temperature and pressure of the LCO_2 are reduced, with the pressure dropping to 659 kPa and the temperature dropping to -50°C. However, partial vaporisation of the LCO_2 will occur at this time, and the vaporisation fraction is related to the temperature difference between node C-4 and node C-5. The temperature between node C-5 is set at -50°C, so the value of the vaporisation fraction is determined by the temperature of node C-4. At this time, the proportion of LCO_2 is called the liquefaction fraction rate of CO_2 BOG. Taking the 85% ship working condition as an example, the relationship between the compressor power and the liquefaction fraction of CO_2 BOG and the node C-4 temperature under different external ambient temperatures is studied. A summary of the results is shown in Fig. 8.

From Fig. 8 (a)~(e), it can be seen that, with the increase of the node C-4 temperature, the node C-3 pressure and the power of Compressor-1 gradually increase, while the liquefaction fraction of CO_2 BOG gradually decreases. This is because, as the temperature of node C-4 increases, the liquefaction temperature of the CO_2 and the corresponding liquefaction pressure also increase gradually. Therefore, the pressure of node C-3 and the power of Compressor-1 increase gradually. At the same time, the temperature and pressure of node C-4 increase, but the temperature and pressure of node C-5 are set and unchanged, so the difference between the temperature and pressure of node C-4 and node C-5 increases, resulting in an increase in the vaporisation fraction of CO_2 BOG and a decrease in the liquefaction fraction. By comparing Fig. 8 (a)~(e), it can be found that, under the same ship working condition, the liquefaction fraction gradually decreases and the compressor power consumption gradually increases with the increase of the ambient temperature. This is because, with the increase of the ambient temperature, the temperature difference between the LCO_2 storage tank and the ambient environment becomes larger, so the infiltration heat increases and the amount of CO_2 BOG also increases; the cold energy required for reliquefaction of the CO_2 BOG also increases, but the working conditions of the ship remain unchanged, and the

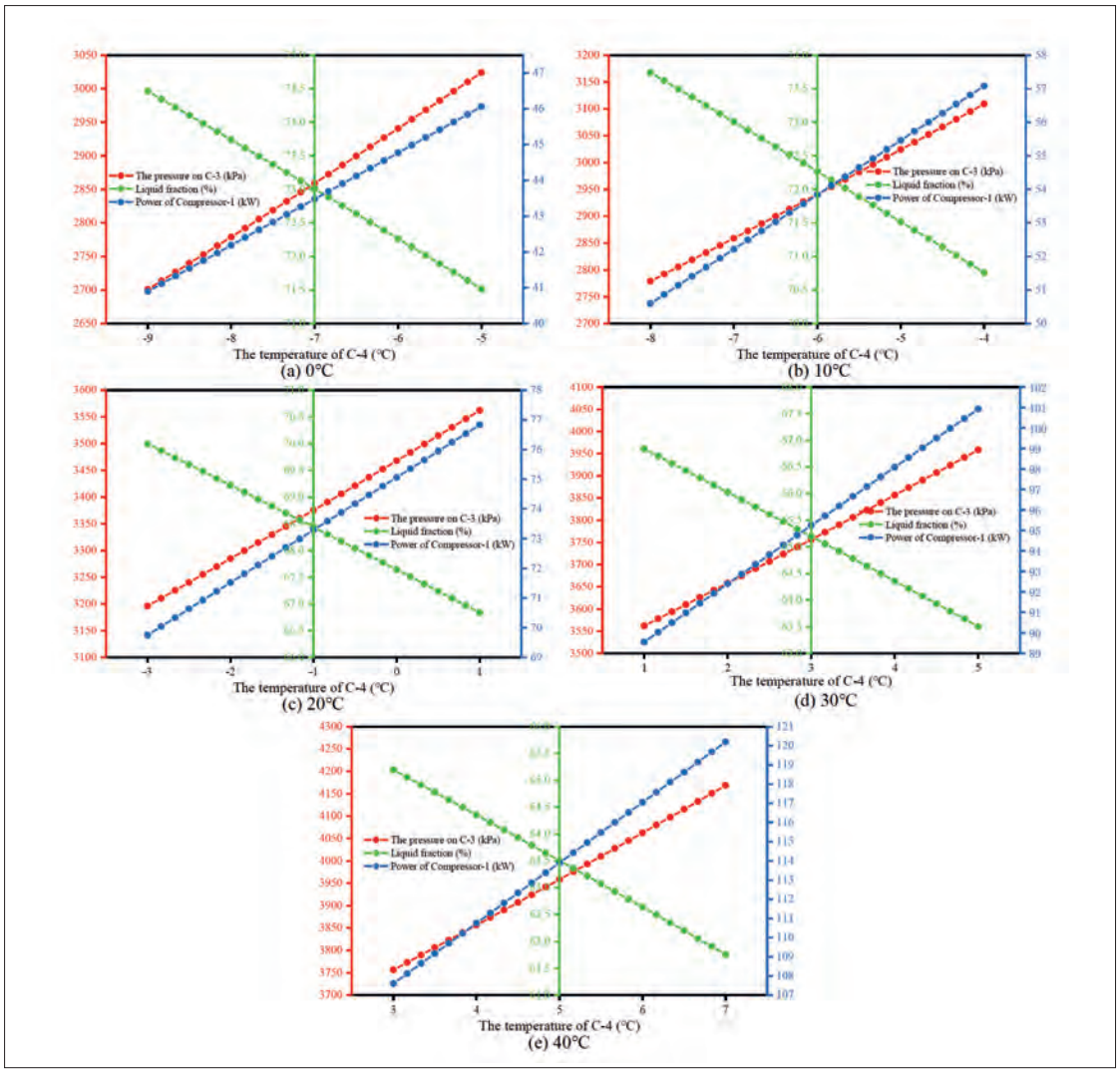

Fig. 8. The relationship between compressor power consumption, CO_2 BOG liquid fraction and node C-4 at different ambient temperatures

amount of liquid ammonia consumed per hour is also basically unchanged, so the maximum cold energy released by the system is constant. In order to ensure that temperature crossing does not occur in the normal operation of Heater-1, the higher the ambient temperature is, the higher the temperature setting of node C-4 is. As a result, the liquefaction temperature of CO_2 and the liquefaction pressure increase, as do the pressure of node C-3 and the power of Compressor-1, and the corresponding liquefaction fraction decreases. Under 85% conditions, when the ambient temperature is 0°C and the node C-4 temperature is -9°C, the liquid fraction of CO_2 BOG is the maximum, at 74.46%, and the power of Compressor-1 is the minimum, at 40.90 kW. When the ambient temperature is 40°C and the node C-4 temperature is 7°C, the liquid fraction of CO_2 BOG is the minimum, at 61.76%, and the power of Compressor-1 is the maximum, at 120.2 kW. Under these conditions, when the node C-4 temperature is 3°C, the CO_2 BOG liquefaction fraction is 65.20%, and the power of Compressor-1 is 107.6 kW. In conclusion, reducing the temperature of node C-4 has a positive effect on improving the liquefaction fraction of CO_2 BOG, and also reduces the power consumption of the compressor.

TEMPERATURE DETERMINATION OF NODE C-4

According to the above studies, it can be found that reducing the temperature of node C-4 can increase the heat transfer rate of Heater-1, increase the liquefaction fraction of CO_2 BOG, and reduce the power consumption of the compressor. Therefore, the temperature of node C-4 should be reduced as much as possible in order to ensure the normal operation of the system. Based on this, the lowest temperature of node C-4 under different working conditions and different ambient temperatures of the ship, as well as the liquefaction fraction of CO_2 BOG and the power consumption of the compressor under the temperature of the C-4 node, are summarised in Fig. 9.

From Fig. 9 (a)~(c), it can be seen that with the increase of ambient temperature, the node C-4 temperature and the power consumption of Compressor-1 gradually increase, while the node C-5 liquefaction fraction decreases under the same ship operating condition. This is because, when the ship is under a certain working condition, the amount of ammonia fuel supplied and the cold energy it can release are also certain. As the ambient temperature increases, the amount of CO_2 BOG that needs to be liquefied keeps increasing. Therefore, the temperature of node C-4 keeps rising; that is, the liquefaction temperature of the CO_2 BOG keeps rising, so the liquefaction pressure corresponding to node C-3 and the power consumption of the compressor gradually increase. The liquefied CO_2 BOG is expanded by the V-1 expansion valve, the LCO_2 will partially vaporise, and an increase in the node C-4 temperature increases the pressure and temperature difference between node C-4 and node C-5. Therefore, the vaporisation fraction of node C-5 will increase, resulting in the reduction of the liquefaction fraction of CO_2 BOG.

From Fig. 9 (a)~(c), it can also be seen that, at the same ambient temperature, the node C-4 temperature and the power consumption of Compressor-1 gradually decrease or remain unchanged, while the node C-5 liquefaction fraction increases or remains unchanged with the increase of ship operating conditions. This is because, when the ambient temperature remains unchanged, the amount of CO_2 BOG that needs to be liquefied remains unchanged. With the increase of the ship working conditions, the liquid ammonia supply and the cold energy that can be released by the system keep increasing.

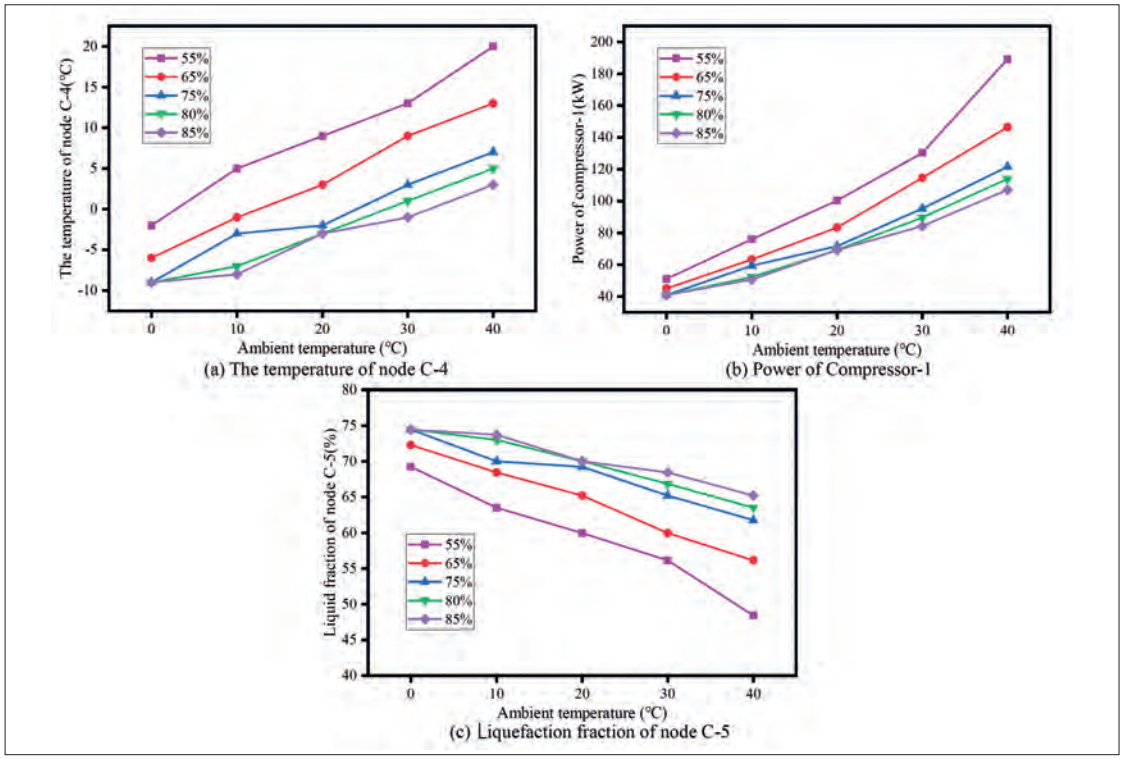

Fig. 9 Variation relationship between main parameters and ambient temperature under different working conditions

Therefore, the temperature of node C-4 keeps decreasing; that is, the liquefaction temperature of the CO_2 BOG decreases and the corresponding liquefaction pressure also decreases. As a result, the power consumption of Compressor-1 decreases gradually, and the temperature difference and pressure difference between node C-4 and node C-5 decrease gradually. After expansion in the expansion valve V-1, the LCO_2 vapour fraction decreases gradually, so the liquefaction fraction increases gradually.

At the same ambient temperature, the node C-4 temperature and the power consumption of Compressor-1 are the minimum when the ship working condition is 85%, and node C-5 has the maximum liquefaction fraction. Taking 85% as an example, when the ambient temperature is 0°C, the node C-4 temperature is -9°C, and the power consumption of Compressor-1 and the liquefaction fraction of node C-5 are 40.81 kW and 74.46%, respectively. When the ambient temperature is 10°C and the node C-4 temperature is -8°C, the power consumption of Compressor-1 and the liquefaction fraction of node C-5 are 50.56 kW and 73.74%, respectively. When the ambient temperature is 20°C and the node C-4 temperature is -3°C, the power consumption of Compressor-1 and the liquefaction fraction of node C-5 are 69.24 kW and 70%, respectively. When the ambient temperature is 30°C, the node C-4 temperature is -1°C, and the power consumption and liquefaction fraction of node C-5 are 84.18 kW and 68.44%, respectively. When the ambient temperature is 40°C and the node C-4 temperature is 3°C, the power consumption of Compressor-1 and the liquefaction fraction of node C-5 are 107.1 kW and 65.2%, respectively.

EXERGY EFFICIENCY ANALYSIS

Exergy of logistics

Assume that the medium of the system is stable flow. For the stable flow system:

$$E_{x,mass} = m[(h - h_0) - T_0(s - s_0)] \quad (5)$$

In the formula, m is the mass flow of the medium; h and s are the specific enthalpy and specific entropy of each medium, respectively.

Exergy efficiency calculation

Exergy efficiency can be used as an important index to evaluate the ability of a system to do external work [38]. In this study, the exergy efficiency can be reflected in the utilisation of liquid ammonia cold energy in the CO_2 BOG reliquefaction system. The exergy efficiency η is equal to the ratio of revenue exergy to payout exergy. The exergy efficiency of each device can be calculated to get the exergy efficiency of the whole system.

(1) Exergy efficiency of heat exchanger

$$\eta_H = \frac{E_{x,in}}{E_{x,p}} \times 100\% \quad (6)$$

In the formula,

$E_{x,in}$ is the revenue exergy, $E_{x,p}$ is the payout exergy.

The revenue exergy of heat-exchanger Heater-1 is the difference between the import exergy and exit exergy of the heat logistics, while the payout exergy is the difference between the exit exergy and import exergy of the cold logistics. The revenue exergy of heat exchanger Heater-2 is the difference between the exit exergy and import exergy of the cold logistics, while the payout exergy is the difference between the import exergy and exit exergy of the heat logistics.

(2) Exergy efficiency of compressor

The exergy efficiency of the compressor is the ratio of the effective revenue exergy $E_{x,c}$ of a compressor to the power P_C of the compressor. The exergy efficiency of the compressor is as follows:

$$\eta_C = \frac{E_{x,c}}{P_C} \times 100\% \quad (7)$$

The effective revenue exergy $E_{x,c}$ of compressor is the difference between the exit exergy and import exergy of the compressor.

(3) Exergy efficiency of pump

The exergy efficiency of the pump is the ratio of effective power consumption E_{xefc} to the pump power P, and is as follows:

$$\eta = \frac{E_{xeft}}{P} \times 100\% \quad (8)$$

The effective power consumption of the pump E_{xefc} is the difference between the exit exergy and import exergy.

(4) Exergy efficiency of the system

The exergy efficiency of the system is the ratio of the sum of the effective revenue exergy to the sum of the payout exergy in the system, and the calculation formula is as follows:

$$\eta = \frac{\sum E_{x,in}}{\sum E_{x,p}} \times 100\% \quad (9)$$

In the formula,

$$\sum E_{x,in} = E_{x,in} + E_{x,c} + E_{xeft} \quad (10)$$

$$\sum E_{x,p} = E_{x,p} + P_C + P \quad (11)$$

The exergy efficiency of the different equipment and the whole system can be calculated in 55%, 65%, 75%, 80%, and 85% working conditions and in different ambient temperatures according to Eqs. (5)~(11), and is shown in Fig. 10.

The exergy efficiency of Heater-1 mainly represents the effect of the utilisation of cold energy in the system. As can be seen from Fig. 10 (a), the exergy efficiency of Heater-1 decreased gradually with the increase of the ambient temperature, which is because the exergy efficiency of the heat exchanger is mainly related to the heat exchange temperature difference. As can be seen from Fig. 9, with the increase of the ambient temperature, the temperature of node C-4 keeps rising. It can also be seen from Fig. 7 that, as the temperature of node C-4 rises, the LMTD of Heater-1 gradually rises, so the exergy loss of the heat exchanger increases and the exergy efficiency decreases. It can also be seen from Fig. 10 (a) that, under the same ambient temperature, the exergy efficiency of Heater-1 increases with the increase of the ship working conditions. This is because the higher the ship working

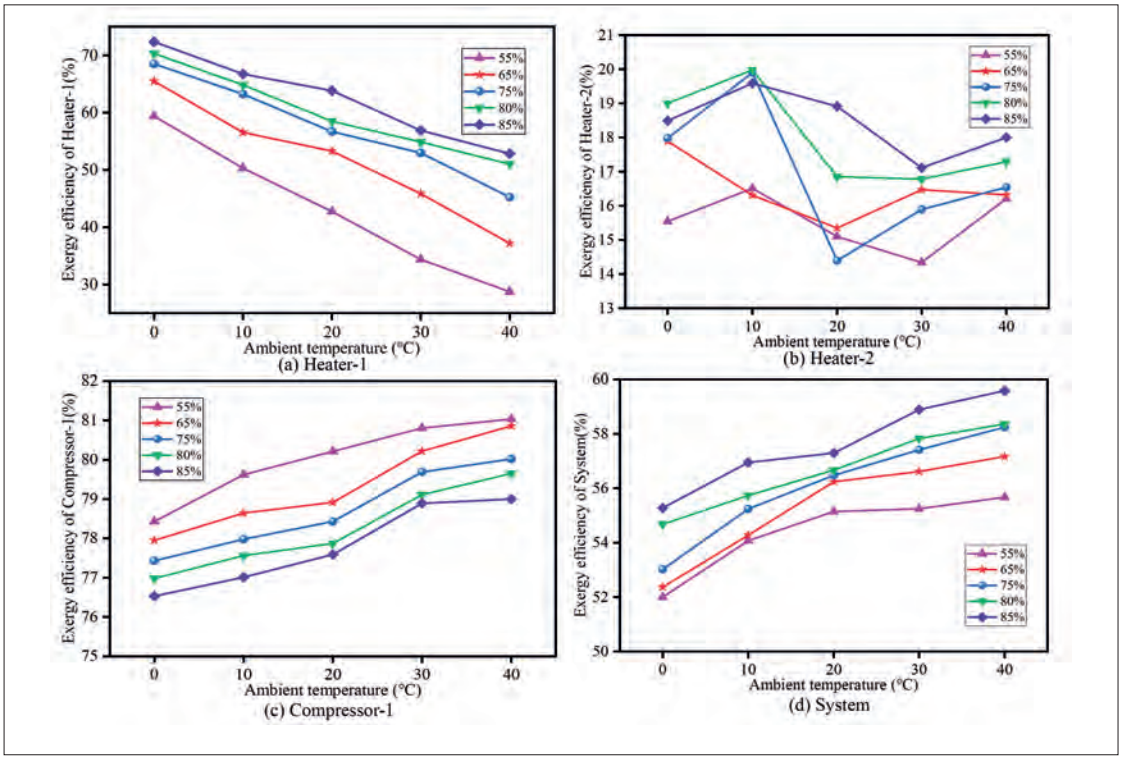

Fig. 10. Exergy efficiency of different devices and system

conditions, the greater the ammonia fuel supply, the richer the cold energy released, and the lower the minimum temperature that node C-4 can achieve. As the LMTD of Heater-1 becomes smaller, its exergy loss will decrease and the exergy efficiency will increase. When the ship working condition is 55% and the ambient temperature is 40°C, the exergy efficiency of Heater-1 is the lowest, at 28.71%; when the ship working condition is 85% and the ambient temperature is 0°C, the exergy efficiency of Heater-1 is the highest, at 72.36%. As can be seen from Fig. 10 (d), when the ship working condition is 85% and the ambient temperature is 0°C, the exergy efficiency of the system is the least, reaching 51.99%. When the ship working condition is 85% and the ambient temperature is 40°C, the exergy efficiency of the system reaches the maximum, which is 59.58%. Therefore, the system proposed in this study could effectively utilise the cold energy of liquid ammonia.

CONCLUSIONS

To address the problems of the waste of liquid ammonia cold energy and the high power consumption in the CO_2 BOG reliquefaction process of ammonia-powered CO_2 carriers, a CO_2 BOG reliquefaction system using liquid ammonia cold energy is proposed. The main conclusions are as follows:

1. A CO_2 BOG reliquefaction system with liquid ammonia as the cold source is designed. Under the same conditions, compared with the existing reliquefaction technology, Aspen HYSYS simulation software is used to establish the process and simulate two systems. The compressor power consumption of the two systems is 102.03 kW and 71.67 kW, respectively. It can be seen that the use of liquid ammonia cold energy can greatly reduce the compressor power consumption in the process of CO_2 BOG reliquefaction.
2. In order to reduce the compressor power consumption and improve the liquefaction fraction of CO_2 BOG, the node C-4 temperature is optimised and analysed. The results show that, with the increase of the external temperature, the node C-4 temperature and the power consumption of Compressor-1 gradually increase, while the liquefaction fraction of CO_2 BOG decreases. At the same external temperature, the node C-4 temperature and the power consumption of Compressor-1 decrease with the increase of ship operating conditions, while the liquefaction fraction of CO_2 BOG increases; thus, the optimal temperature values of node C-4 in the system under different working conditions are determined. The maximum CO_2 BOG liquefaction fraction after optimisation is 74.46%, and the minimum value of compressor power is 40.81 kW.
3. The exergy efficiency models of the main equipment and the system are established. It is found that, with the increase of the external temperature, the exergy efficiency of Heater-1 decreases gradually. At the same external temperature, the exergy efficiency of Heater-1 increases gradually with the increase of ship working conditions, while the exergy efficiency of the whole system decreases gradually with the increase of the external temperature. The maximum exergy efficiency value of Heater-1 is 72.36%, and the maximum exergy efficiency value of the whole system is 59.58%.
4. In view of this, the CO_2 BOG reliquefaction system using liquid ammonia fuel cold energy proposed in this study

solves the problems of the waste of liquid ammonia cold energy and the high power consumption in the CO_2 BOG reliquefaction process of ammonia-powered CO_2 carriers. This provides a new form of fuel cold energy utilisation for ammonia-powered ships in the future and promotes the development of energy-saving and emission reduction technologies for ships.

ACKNOWLEDGEMENT

This project was funded by the Natural Science Foundation of Shandong Province of China (ZR2021ME156).

REFERENCES

1. M. Bui, C. S. Adjiman, A. Bardow, E. J. Anthony, A. Boston, S. Brown, and N. MacDowell, "Carbon capture and storage (CCS): the way forward," *Energy & Environmental Science*, vol. 11, no. 5, pp. 1062-1176, 2018, doi: 10.1039/C7EE02342A.

2. E. S. P. Aradóttir, H. Sigurdardóttir, B. Sigfússon, and E. Gunnlaugsson, "CarbFix: a CCS pilot project imitating and accelerating natural CO_2 sequestration," *Greenhouse Gases: Science and Technology*, vol. 1, no. 2, pp. 105-118, 2011, doi: 10.1002/ghg.18.

3. K. Onarheim, A. Mathisen, and A. Arasto, "Barriers and opportunities for application of CCS in Nordic industry–A sectorial approach," *International Journal of Greenhouse Gas Control*, vol. 36, pp. 93-105, 2015, doi: 10.1016/j.ijggc.2015.02.009.

4. P. Mekala, M. Busch, D. Mech, R. S. Patel, and J. S. Sangwai, "Effect of silica sand size on the formation kinetics of CO_2 hydrate in porous media in the presence of pure water and seawater relevant for CO_2 sequestration," *Journal of Petroleum Science and Engineering*, vol. 122, pp. 1-9, 2014, doi: 10.1016/j.petrol.2014.08.017.

5. G. Hegerland, T. Jørgensen, and J. O. Pande, "Liquefaction and handling of large amounts of CO_2 for EOR," *Proc. Seventh International Conference on Greenhouse Gas Control Technologies*, vol. 2, pp. 2541–2544, 2005, doi: 10.1016/B978-008044704-9/50369-4.

6. D. E. Clark, E. H. Oelkers, I. Gunnarsson, B. Sigfússon, S. Ó. Snæbjörnsdóttir, E. S. Aradóttir, and S. R. Gíslason, "CarbFix2: CO_2 and H_2S mineralization during 3.5 years of continuous injection into basaltic rocks at more than 250°C," *Geochimica et Cosmochimica Acta*, vol. 279, pp. 45-66, 2020, doi: 10.1016/j.gca.2020.03.039.

7. H. Wu, R. S. Jayne, R. J. Bodnar, and R. M. Pollyea, "Simulation of CO_2 mineral trapping and permeability alteration in fractured basalt: Implications for geologic carbon sequestration in mafic reservoirs," *International Journal of Greenhouse Gas Control*, vol. 109, p. 103383, 2021, doi: 10.1016/j.ijggc.2021.103383.

8. T. M. P. Ratouis, S. Ó. Snæbjörnsdóttir, M. J. Voigt, B. Sigfússon, G. Gunnarsson, E. S. Aradóttir, and V. Hjörleifsdóttir, "Carbfix 2: A transport model of long-term CO_2 and H_2S injection into basaltic rocks at Hellisheidi, SW-Iceland," *International Journal of Greenhouse Gas Control*, vol. 114, p. 103586, 2022, doi: 10.1016/j.ijggc.2022.103586.

9. H. A. Baroudi, A. Awoyomi, K. Patchigolla, K. Jonnalagadda, and E. J. Anthony, "A review of large-scale CO_2 shipping and marine emissions management for carbon capture, utilisation and storage," *Applied Energy*, vol. 287, p. 116510, 2021, doi: 10.1016/j.apenergy.2021.116510.

10. S. Trædal, J. H. J. Stang, I. Snustad, M. V. Johansson, and D. Berstad, "CO_2 liquefaction close to the triple point pressure," *Energies*, vol. 14, p. 8220, 2021, doi: 10.3390/en14248220.

11. S. H. Jeon and M. S. Kim, "Compressor selection methods for multi-stage re-liquefaction system of liquefied CO_2 transport ship for CCS," *Applied Thermal Engineering*, vol. 82, pp. 360-367, 2015, doi: 10.1016/j.applthermaleng.2015.02.080.

12. J. R. Gómez, M. R. Gómez, R. F. Garcia, and A. D. Catoira, "On board LNG reliquefaction technology: a comparative study," *Polish Maritime Research*, vol. 21, pp. 77-88, 2013, doi: 10.2478/pomr-2014-0011.

13. A. Alabdulkarem, Y. H. Wang, and R. Radermacher, "Development of CO_2 liquefaction cycles for CO_2 sequestration," *Applied Thermal Engineering*, vol. 33, pp. 144-156, 2012, doi: 10.1016/j.applthermaleng.2011.09.027.

14. K. Aliyon, M. Mehrpooya, and A. Hajinezhad, "Comparison of different CO_2 liquefaction processes and exergoeconomic evaluation of integrated CO_2 liquefaction and absorption refrigeration system," *Energy Conversion and Management*, vol. 211, p. 112752, 2020, doi: 10.1016/j.enconman.2020.112752.

15. L. E. Øi, N. Eldrup, U. Adhikari, M. H. Bentsen, J. L. Badalge, and S. Yang, "Simulation and cost comparison of CO_2 liquefaction," *Energy Procedia*, vol. 86, pp. 500-510, 2016, doi: 10.1016/j.egypro.2016.01.051.

16. Y. Sen, H. You, S. Lee, C. Huh, and D. Chang, "Evaluation of CO_2 liquefaction processes for ship-based carbon capture and storage (CCS) in terms of life cycle cost (LCC) considering availability," *International Journal of Greenhouse Gas Control*, vol. 35, pp. 1-12, 2015, doi: 10.1016/j.ijggc.2015.01.006.

17. S. Decarre, J. Berthiaud, N. Butin, and J. L. Guillaume-Combecave, "CO_2 maritime transportation," *International Journal of Greenhouse Gas Control*, vol. 4, no. 5, pp. 857-864, 2010, doi: 10.1016/j.ijggc.2010.05.005.

18. L. Duan, X. Chen, and Y. Yang, "Study on a novel process for CO_2 compression and liquefaction integrated with the refrigeration process," *International Journal of Energy Research*, vol. 37, pp. 1453-1464, 2013, doi: 10.1002/er.2951.

19. U. Zahid, J. An, U. Lee, S. P. Choi, and C. Han, "Techno-economic assessment of CO_2 liquefaction for ship transportation," *Greenhouse Gases: Science and Technology*, vol. 4, no. 6, pp. 734-749, 2015, doi: 10.1002/ghg.1439.

20. A. Awoyomi, K. Patchigolla, and E. J. Anthony, "CO_2/SO_2 emission reduction in CO_2 shipping infrastructure," *International Journal of Greenhouse Gas Control*, vol. 88, pp. 57-70, 2019, doi: 10.1016/j.ijggc.2019.05.011.

21. H. J. Sang and S. K. Min, "Effects of impurities on re-liquefaction system of liquefied CO_2 transport ship for CCS," *International Journal of Greenhouse Gas Control*, vol. 43, no. 2, pp. 225-232, 2015, doi: 10.1016/j.ijggc.2015.10.011.

22. H. Deng, S. Roussanaly, and G. Skaugen, "Techno-economic analyses of CO_2 liquefaction: Impact of product pressure and impurities," *International Journal of Refrigeration*, vol. 103, pp. 301-315, 2019, doi: 10.1016/j.ijrefrig.2019.04.011.

23. Y. Lee, K. H. Baek, S. Lee, K. Cha, and C. Han, "Design of boil-off CO_2 re-liquefaction processes for a large-scale liquid CO_2 transport ship," *International Journal of Greenhouse Gas Control*, vol. 67, pp. 93-102, 2017, doi: 10.1016/j.ijggc.2017.10.008.

24. H. A. Muhammad, C. Roh, J. Cho, Z. Rehman, H. Sultan, Y. J. Baik, and B. Lee, "A comprehensive thermodynamic performance assessment of CO_2 liquefaction and pressurization system using a heat pump for carbon capture and storage (CCS) process," *Energy Conversion and Management*, vol. 206, p. 112489, 2020, doi: 10.1016/j.enconman.2020.112489.

25. J. Kropiwnicki, "Application of Stirling engine type alpha powered by the recovery energy on vessels," *Polish Maritime Research*, vol. 27, no. 1, pp. 96-106, 2020, doi: 10.2478/pomr-2020-0010.

26. H. P. Nguyen, A. T. Hoang, S. Nizetic, X. P. Nguyen, A. T. Le, C. N. Luong, V. D. Chu, and V. V. Pham, "The electric propulsion system as a green solution for management strategy of CO_2 emission in ocean shipping: A comprehensive review," *International Transactions on Electrical Energy Systems*, vol. 31, E12580, 2020, doi: 10.1002/2050-7038.12580.

27. L. C. Law, B. Foscoli, E. Mastorakos, and S. Evans, "A comparison of alternative fuels for shipping in terms of lifecycle energy and cost," *Energies*, vol. 14, no. 24, p. 8502, 2021, doi: 10.3390/en14248502.

28. N. R. Sharma, D. Dimitrios, A. I. Olcer, and N. Nikitakos, "LNG a clean fuel – the underlying potential to improve thermal efficiency," *Journal of Marine Engineering and Technology*, vol. 21, pp. 111-124, 2020, doi: 10.1080/20464177.2020.1827491.

29. M. Comotti and S. Frigo, "Hydrogen generation system for ammonia-hydrogen fuelled internal combustion engines," *International Journal of Hydrogen Energy*, vol. 40, no. 33, pp. 10673-10686, 2015, doi: 10.1016/j.ijhydene.2015.06.080.

30. S. Frankl, S. Gleis, S. Karmann, M. Prager and G. Wachtmeister, "Investigation of ammonia and hydrogen as CO_2-free fuels for heavy duty engines using a high pressure dual fuel combustion process," *International Journal of Engine Research*, vol. 22, no. 10, pp. 3196-3208, 2021, doi: 10.1177/1468087420967873.

31. C. Mounaïm-Rousselle, P. Bréquigny, C. Dumand, and S. Houillé, "Operating limits for ammonia fuel spark-ignition engine," *Energies*, vol. 14, no. 14, p. 4141, 2021, doi: 10.3390/en14144141.

32. A. Valera-Medina, F. Amer-Hatem, A. K. Azad, I. C. Dedoussi, M. D. Joannon, R. X. Fernandes, P. Glarborg, H. Hashemi, X. He, S. Mashruk, J. McGowan, C. Mounaim-Rouselle, A. Ortiz-Prado, A. Ortiz-Valera, I. Rossetti, B. Shu, M. Yehia, H. Xiao, and M. Costa, "Review on ammonia as a potential fuel: From synthesis to economics," *Energy and Fuels*, vol. 35, pp. 6964-7029, 2021, doi: 10.1021/acs.energyfuels.0c03685.

33. H. Li and J. Yan, "Evaluating cubic equations of state for calculation of vapor–liquid equilibrium of CO_2 and CO_2-mixtures for CO_2 capture and storage processes," *Applied Energy*, vol. 86, no. 6, pp. 826-836, 2009, doi: 10.1016/j.apenergy.2008.05.018.

34. U. Lee, S. Yang, Y. S. Jeong, Y. Lim, C. S. Lee, and C. Han, "Carbon dioxide liquefaction process for ship transportation," *Industrial and Engineering Chemistry Research*, vol. 51, no. 46, pp. 15122-15131, 2012, doi: 10.1021/ie300431z.

35. F. Engel and A. Kather, "Improvements on the liquefaction of a pipeline CO_2 stream for ship transport," *International Journal of Greenhouse Gas Control*, vol. 72, pp. 214-221, 2018, doi: 10.1016/j.ijggc.2018.03.010.

36. Y. Shi, J. Shen, D. Qiu, and T. Qin, "Thermal analysis of type C independent tank," *Ships and Ocean Engineering*, vol. 36, no. 3, p. 5, 2020, doi: 10.14056/j.cnki.naoe.2020.03.001.

37. B. Y. Yoo, "The development and comparison of CO_2 BOG re-liquefaction processes for LNG fueled CO_2 carriers," *Energy*, vol. 127, pp. 186-197, 2017, doi: 10.1016/j.energy.2017.03.073.

38. Y. Li, B. Li, F. Deng, Q. Yang, and B. Zhang, "Research on the application of cold energy of largescale LNG-powered container ships to refrigerated containers," *Polish Maritime Research*, vol. 28, no. 4, pp. 107-121, 2022, doi: 10.2478/pomr-2021-0053.